Measurement of transition radiation from medium-energy electrons

M. A. Piestrup, J. O. Kephart, H. Park, R. K. Klein, and R. H. Pantell
Department of Electrical Engineering, Stanford University, Stanford, California 94305

P. J. Ebert, M. J. Moran, and B. A. Dahling
Lawrence Livermore National Laboratory, University of California, Livermore, California 94550

B. L. Berman
Lawrence Livermore National Laboratory, University of California, Livermore, California 94550
and Department of Physics, George Washington University, Washington, D.C. 20052
(Received 19 February 1985)

The absolute differential production efficiencies (photons/eV sr electron) for x rays emitted from each of three transition radiators were measured for incident electron-beam energies of 17.2, 25, and 54 MeV. The radiators were made of stacks of 1.0-μm-thick foils: 18 foils of beryllium, 18 foils of carbon, and 30 foils of aluminum. The radiation spectra were most intense between 0.5 and 2.5 keV, peaking at 0.8, 1.3, and 1.3 keV, respectively. The angular distribution of the transition radiation from the beryllium-foil stack was measured for the three electron-beam energies and found to agree well with theoretical predictions. Owing to K-shell absorption, the photon-energy spectra from the carbon and aluminum stacks are narrowed. Theoretical calculations, which include both the two-surface interference and photon attenuation in the foil material, agree well with these data. A method of enhancing output using a split-foil stack is considered; cursory experiments with a split stack of Mylar foils showed enhanced emission. The use of transition radiation as a source of x rays for lithographic purposes may be practical.

I. INTRODUCTION

Transition radiation,[1-3] the production of photons when charged particles cross the interface between two media, has been applied to high-energy particle detection because the total x-ray output is directly proportional to the energy of the particle.[4] Indeed, a number of experiments have been conducted with periodic radiators and ultrarelativistic electrons.[5-7] In recent work it has been shown that medium-energy electrons (10—100 MeV) generate transition-radiation spectra that are rich in 0.9—5-keV x rays. However, in these measurements[8-11] only the relative photon intensities were measured and the lowest electron-beam energy was 66 MeV. With the rationale of performing absolute measurements of the differential production efficiencies at lower electron energies, we have conducted experiments with multiple-foil targets of beryllium, carbon, and aluminum with 17.2-, 25-, and 54-MeV electrons at the Lawrence Livermore National Laboratory Electron-Positron Linear Accelerator. The measured spectra and angular distributions for the stated conditions are in agreement with theoretical calculations. A brief account of one aspect of this work (the confirmation of interference at the interfaces of a single foil) has been published elsewhere.[12]

The transition radiation produced per electron is at least 2 orders of magnitude greater than for synchrotron radiation. Electrons of relatively low energy ($5 < E < 50$ MeV) can produce transition radiation, whereas greater currents of much-higher-energy electrons are needed to produce an equivalent amount of synchrotron radiation at the same wavelength. Because of the efficiency of transition-radiation production and the availability of medium-energy electron sources, applications in areas such as x-ray lithography, microscopy, and ultrafast relaxation processes appear to be very attractive. Over a restricted energy range, the peak spectral brilliance (photons/s mm^2 mrad^2 eV) of a transition-radiation source produced by a linear accelerator (linac) with subharmonic bunching (with $\simeq$20-ps beam bursts of several hundred amperes peak current) rivals that of a synchrotron bend-magnet source.

II. THEORETICAL PROPERTIES OF TRANSITION RADIATION

A. Differential production efficiency

The theory of transition radiation was first reported by Ginzburg and Frank,[1] with further developments by Garibian[2] and Ter-Mikaelian.[3] Excellent descriptions of transition-radiation properties for ultrarelativistic electrons ($E > 1$ GeV) are given by Ter-Mikaelian and Cherry *et al.*[13,14] The following parallels their descriptions. While the transition-radiation formulas are rather complicated, some properties can be deduced by inspection of limiting cases.

Transition radiation occurs when a moving charged particle encounters a sudden change in dielectric constant at the interface between dissimilar media (e.g., between a vacuum and a solid). Ordinarily, a particle which moves with constant velocity does not radiate unless it is in a re-

fractive medium and the particle velocity is equal to the phase velocity of an electromagnetic wave along the direction of motion—as is the case for Čerenkov radiation. However, if the interaction length is limited, or equivalently, if the dielectric constant changes suddenly, then velocity matching is not necessary. The minimum distance over which an electromagnetic wave and a charged particle can exchange energy is called the formation length and is given by

$$Z_i = \frac{2\beta c}{\omega[1-\beta(\epsilon_i - \sin^2\theta)^{1/2}]} , \tag{1}$$

where $\gamma=(1-\beta^2)^{-1/2}$, $\epsilon_i=1-(\omega_i/\omega)^2$ $(i=1,2)$ are the permittivities of the two media, ω_i are their respective plasma frequencies, $\hbar\omega$ is the photon energy, $\beta=v/c$, v is the speed of the electron, c is the speed of light, and θ is the angle of emission. mks units are used in this paper.

For relativistic electrons $\beta\simeq 1$ and $\sin\theta\simeq\theta$, so that

$$Z_i \simeq \frac{4\beta\lambda\!\!\!^{-}}{(1/\gamma)^2+\theta^2+(\omega_i/\omega)^2} , \tag{2}$$

where $\lambda\!\!\!^{-}=c/\omega$. In this paper, $\omega<5$ keV and $Z_2\simeq 1$ μm. As will be seen later, it is important for the foils to be thin so that x rays are not strongly absorbed.

In traversing the interface, the number of photons per unit time emitted by an electron is proportional to the dot product of the particle velocity and the electric field strength. For a single interface Ginzburg and Frank[1] calculate the differential production efficiency for transition radiation as

$$\frac{d^2N_0}{d\Omega\, d\omega} = \left[\frac{\alpha\omega\sin^2\theta}{16\pi^2c^2}\right](Z_1-Z_2)^2 , \tag{3}$$

where the fine-structure constant $\alpha=\frac{1}{137}$ and Z_1 and Z_2 are given by Eq. (1).

From Eq. (3), transition radiation from an electron crossing a single interface is most intense at $\theta_{\rm opt}$, the apex angle of a cone given by[10]

$$\theta_{\rm opt}\simeq\tfrac{1}{3}\{[(\delta_1+\delta_2)^2+12\delta_1\delta_2]^{1/2}-(\delta_1+\delta_2)\} , \tag{4}$$

where $\delta_i=[(1/\gamma)^2+(\omega_i/\omega)^2]/2$ $(i=1,2)$. In general, $\omega_2\gg\omega_1$, where ω_1 is the plasma frequency of the medium in which the foils are immersed. For the case of a foil stack in vacuum, $\omega_1=0$ and $\theta_{\rm opt}\simeq 1/\gamma$. This is illustrated schematically in Fig. 1, which, for the purposes of clarity, exaggerates the size of the angle.

For a single electron crossing M foils ($2M$ interfaces), each of thickness l_2 and each separated by a spacing l_1, the differential production efficiency is[10–12]

$$\frac{d^2N}{d\Omega\, d\omega} = \left[\frac{d^2N_0}{d\Omega\, d\omega}\right]4\sin^2(l_2/Z_2)F(M,X) , \tag{5}$$

where

$$F(M,X)=\frac{1+\exp(-M\sigma)-2\exp(-M\sigma/2)\cos(2MX)}{1+\exp(-\sigma)-2\exp(-\sigma/2)\cos(2X)} \tag{6}$$

and $\sigma=\mu_1 l_1+\mu_2 l_2$, $X=l_1/Z_1+l_2/Z_2$, and μ_1 and μ_2 are the linear absorption coefficients of the spacing and foil media, respectively ($\mu_1=0$ for vacuum spacing).

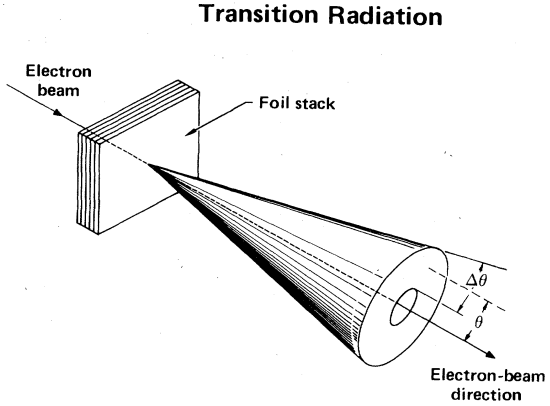

FIG. 1. Schematic diagram of the transition-radiation cone produced by a relativistic electron beam passing through a stack of foils. The size of the cone angle is exaggerated for clarity. For an incident electron energy of 54 MeV, $\theta\simeq\Delta\theta\simeq 1/\gamma=9.3$ mrad.

Note that the second term in Eq. (5), $4\sin^2(l_2/Z_2)$, accounts for coherent addition of amplitudes from the two interfaces of a single foil and gives a peak value twice as large as from two interfaces when the emission is completely random. This occurs when there is constructive interference between the waves generated at the front and back (upstream and downstream) interfaces.[11–17] The radiation intensity is maximized when the thickness of the foil is such that both the electron and the photon travel an integral number of wavelengths in the field generated at the first interface.

At high photon energies, where x-ray absorption is small or negligible ($\sigma\simeq 0$),

$$F(M,X)\simeq\frac{\sin^2(MX)}{\sin^2 X} . \tag{7}$$

When the spacing between the foils l_1 exceeds the formation length of the gap material Z_1, $F(M,X)$ varies rapidly compared with the single-interface term given by Eq. (3), and the peak spectral intensity is found to vary as the square of the number of interfaces when $X=n\pi$ and n is an integer.

When the intensity varies rapidly with both photon energy and angle [see Eq. (7)], the radiation maxima might be difficult to resolve. These variations are averaged when the detector has low resolution in both solid angle and energy. In addition, the angular distribution is broadened because of both the finite electron-beam dimensions and multiple scattering. When the periods of $F(M,X)$ are not experimentally resolvable and the absorption of the emitted radiation in the foil material is not negligible, Eq. (6) becomes

$$\langle F(M,X)\rangle\simeq\frac{1-\exp(-M\sigma)}{\sigma} . \tag{8}$$

Equation (5) now can be written as

$$\frac{d^2N}{d\Omega\, d\omega} \simeq \left[\frac{\alpha}{\omega}\right] \frac{1-\exp(-M\sigma)}{\sigma} \left[\frac{2\beta\omega_2^2}{\pi\omega^2}\right]^2 \frac{\sin^2(l_2/Z_2)\sin^2\theta}{[(1/\gamma)^2+\theta^2]^2[(1/\gamma)^2+\theta^2+(\omega_2/\omega)^2]^2} . \tag{9}$$

We have used this expression for the differential production efficiency in our experimental analysis below.

We see, from Eq. (8), that when $M\sigma \gg 1$ the asymptotic value for F is $1/\sigma(\omega)$ and that beyond $2/\sigma$ foils the radiation intensity cannot be increased significantly by adding more foils. Thus, to optimize 1-keV-photon production from a stack of 1-μm-thick beryllium foils, 16 foils are adequate.

B. Spectral shape

The shape of the transition-radiation spectrum [see Eqs. (5)—(9)] is determined by three main factors: (a) the absorption of the emitted radiation in the foils; (b) the critical photon energy $\hbar\omega_c = \gamma\hbar\omega_2$, above which the spectrum falls off as $(\omega_2/\omega)^4$; and (c) the constructive interference between the two interfaces of single foil. The effect of these three factors is shown in Fig. 2, where the radiation intensity is plotted as a function of photon energy for three cases: (1) for no absorption, (2) for absorption but no single-foil coherence, and (3) for both absorption and single-foil coherence present.

The absorption in the foils results in a reduction of the number of lower-energy photons, while the falloff at the high-energy end of the spectrum is determined by the critical energy $\hbar\omega_c$. Efficient production of photons at a particular energy is dependent on the electron-beam energy, which determines $\hbar\omega_c$. Above this energy, the spectrum is proportional to ω^{-4}. If beryllium, which has a plasma frequency of 24.5 eV, is used, for the critical photon energy to be greater than 1 keV the electron-beam energy must be greater than 20 MeV.

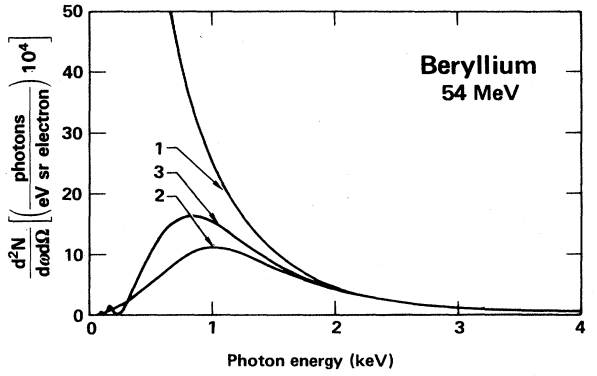

FIG. 2. Calculated differential production efficiency for transition radiation from a single 1 μm beryllium foil (two interfaces) for 54-MeV incident electrons. Three cases are shown: (1) for no absorption, (2) for absorption but no single-foil coherence, and (3) for both absorption and single-foil coherence. Constructive interference of the waves produced at the front and back surfaces of a foil results in an increase in the spectral intensity over the single-interface case. The angle of observation is 9.3 mrad.

Constructive interference between photons from the interfaces of a single foil is expressed by the $\sin^2(l_2/Z_2)$ term in Eq. (9). This gives a factor-of-2 increase in the peak spectral intensity over that for the nonresonant case, where the foil thicknesses are nonuniform.

With absorption, there is a foil thickness for which the photon flux at a given energy is maximized. This feature is illustrated in Fig. 3, where the number M of beryllium foils is kept constant while the foil thickness is varied. Both the photon energy of the spectral peak and its magnitude depend upon foil thickness. However, as can be seen from this figure, the variation in intensity with foil thickness is not very large, and hence the foil thickness can be obtained roughly be setting $l_2 \simeq (\pi/2)Z_2$ in Eq. (1), giving

$$l_2 \simeq \lambda \left[\frac{2}{\gamma^2} + \left[\frac{\omega_2}{\omega}\right]^2\right]^{-1} . \tag{10}$$

Here the angle of emission θ is taken to be $1/\gamma$.

In general, the energy spectra produced by most transition radiators are broad, as shown in Fig. 4(a) for beryllium. There are two ways to obtain narrower spectra. One way is to use the single-foil or multiple-foil coherence effect.[11—17] The other way is to choose the material of the foils so that the spectrum is narrowed due to the sudden change in x-ray absorption at the K photoabsorption edge(s) in the material. This case is illustrated in Fig. 4(c) for aluminum, whose K edge is at 1.56 keV. The increase in absorption above the K edge results in a narrower energy spectrum than would otherwise be observed. If a detector with low-energy resolution were used to detect this radiation (as was the case for the present experiment), then the spectrum would be smoothed, as is shown by the solid curve in Fig. 4(c).

For carbon, which has a K edge at 284 eV, we expect a

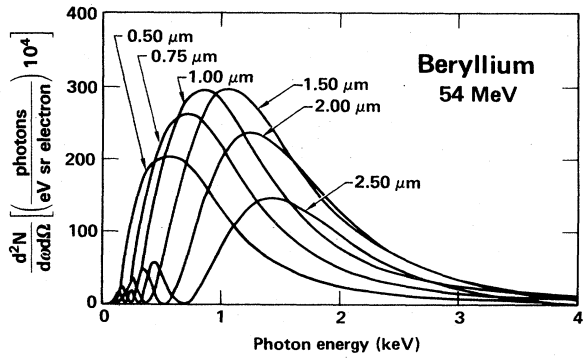

FIG. 3. Calculated spectral distributions from 18 foils of various thicknesses of beryllium. The electron-beam energy is 54 MeV; the spacing between the foils is much larger than the thickness of each foil. The angle of observation is 9.3 mrad. The energy of the spectral peak increases monotonically with foil thickness, whereas the peak intensity reaches a maximum for a foil thickness slightly greater than 1 μm.

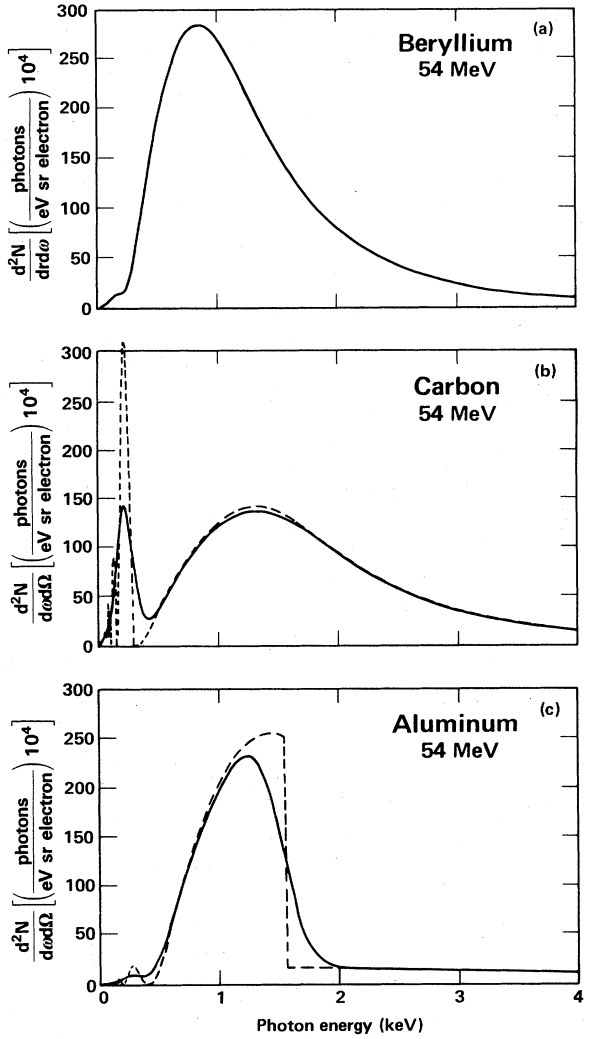

FIG. 4. Calculated effect of K-shell absorption on the transition-radiation spectrum for 54-Mev electrons. Beryllium (a) has no K-shell absorption edge within the energy interval measured here, while carbon and aluminum have K edges at 284 and 1560 eV, respectively. Since there is a large increase in the absorption above the K edge, the carbon (b) and aluminum (c) spectra are altered. The carbon spectrum shows a peak at 270 eV, blow the K edge. The aluminum spectrum is truncated above 1560 eV. The spectra shown by the solid curves include the effect of the detector resolution; the dashed curves do not.

significant decrease in the emergent photon flux just above this energy. The predicted intensity spectrum is shown in Fig. 4(b), where again the spectrum is shown both with and without the energy resolution of the detector taken into account. The decreased photon absorption below the K edge results in a narrow peak at approximately 270 eV.

C. Production efficiency from lower-energy electrons

There are many practical advantages in obtaining transition radiation from electron beams with energy less than 20 MeV. Chief among these is that such sources are available at relatively low cost. Also, medium- or low-energy accelerators can have extremely high peak currents, as is the case of field-emission Marx-bank accelerators.

The differential production efficiency [in photons emitted per unit solid angle, from Eq. (9)] varies roughly as γ^2 for $\omega \ll \gamma\omega_2$, and thus a small change in the electron-beam energy results in a large variation in x-ray output per unit solid angle. In the data presented below the lowest electron-beam energy used was 17.2 MeV. For this case, $\omega \simeq \gamma\omega_2 = 850$ eV, and the differential production efficiency decreases somewhat faster than γ^2.

As compared with the differential production efficiency, the total photon flux varies more slowly with γ. This can be seen by integrating Eq. (3) over solid angle to obtain the number of photons emitted per unit frequency per electron per interface:

$$\frac{dN}{d\omega} \simeq \left[\frac{2\alpha}{\pi\omega}\right]\left[\left[\frac{1}{2}+\frac{1}{b}\right]\ln(1+b)-1\right], \tag{11}$$

where $b=(\gamma\omega_2/\omega)^2$. When $b \gg 1$ ($\omega \ll \gamma\omega_2$), the photon flux per unit frequency [Eq. (11)] is proportional to $\ln\gamma$; thus, a large variation in the electron-beam energy results in a relatively small change in the low-energy photon production efficiency. For relatively low-energy beams, as for the 17.2-MeV case, $\omega \simeq \gamma\omega_2$, and the total photon flux is roughly constant (1.6×10^{-5} photons/10% bandwidth).

The reduced differential production efficiency and the total photon flux from lower electron-beam energies can be offset by the large currents available from low-energy accelerators. The lowest photon-energy peak observed from the carbon-foil stack was at 270 eV. A 5-MeV electron beam could be used to produce this peak because the condition for efficient photon production that $\omega < \gamma\omega_2$ still is satisfied. Since relatively inexpensive high-current field-emission Marx-bank accelerators are available at this energy, high fluxes of soft x rays could be produced.

D. Increasing the intensity of transition radiation

The intensity of transition radiation from a foil stack can be increased by allowing some of the x rays to leave the stack before too many foils are encountered. The number of foils then could be increased, the maximum number now being limited by the multiple scattering of the electrons in the foils. Such a scheme is shown schematically in Fig. 5. The electron beam is steered by approximately one beam diameter into the transverse dimension of the foil stack. The x rays generated in the upper half of the radiation cone will leave the stack, while x rays in the lower half will be emitted largely from the last few foils (of total thickness $2/\sigma$). The spacing between the foils can be adjusted so that the number of foils encountered by a photon in the upper half plane is less than $2/\sigma$. From simple geometric considerations, the spacing between foils should be $l_1 \simeq d/M\theta_{\rm opt} \simeq \sigma\gamma d/2$, where d is the diameter of the electron beam and $l_1 \gg l_2$. For 1-μm-thick beryllium foils, and using a 1-mm-diam,

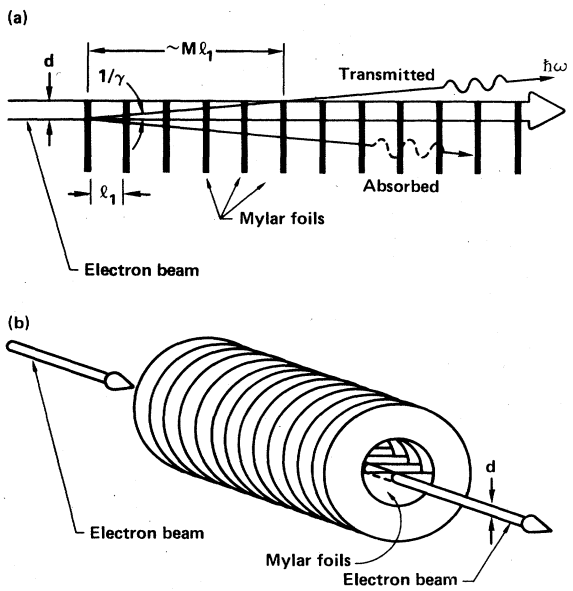

FIG. 5. Transition radiation from a split-foil stack. The electron beam is steered one beam diameter into the transverse dimension of the foil stack. The radiation is enhanced in the upper half plane. The x-rays generated in the upper half of the radiation cone will leave the stack before $M < 2/\sigma$ foils are encountered, while x rays in the lower half will be largely absorbed by the foils. Such a stack was fabricated using 28 foils of 1.5-μm-thick Mylar, as shown in (b). The separation between the foils was 5 mm.

54-MeV electron beam, the minimum spacing between foils in order to allow 1-keV photons to escape would be $\simeq$6 mm.

III. EXPERIMENTAL APPARATUS AND PROCEDURE

Our experiments were performed with the Lawrence Livermore National Laboratory Electron-Positron Linear Accelerator. A schmatic diagram of the experimental apparatus is shown in Fig. 6. The electron beam, after passing through the foil stack, was deflected by a sweeping magnet through an angle of 90° into a 5-m-deep dump hole in the floor. The transition-radiation photons were detected with a gas-flow x-ray proportional counter. Several foil stacks were mounted on a platform that could rotate each of them into the electron beam without the necessity of breaking the vacuum. A ZnS(Au) phosphor target, used for the alignment of the electron beam relative to the target chamber, also was mounted on the rotatable platform.

A 127-μm-thick aluminium foil located downstream from the sweeping magnet (see Fig. 6) could be inserted into the beam pipe to absorb the soft photons generated in the foil stack while still allowing the hard background photons ($\hbar\omega \geq 10$ keV) to be transmitted. This enabled us to measure the background radiation under nearly identical experimental conditions. The background measured in this way was subtracted to obtain the data presented here.

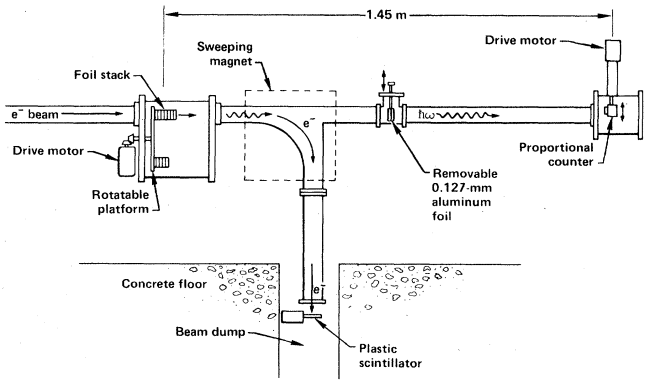

FIG. 6. Schematic diagram of the experimental apparatus. After passing through the foil stack, the electron beam was swept into a beam dump in the floor. The radiation produced in the foils was detected by a proportional counter located 1.45 m from the stack. A 127-μm-thick aluminum foil could be inserted into the photon beam line to attenuate the soft x rays. This made it possible to perform *in situ* background measurements.

The electron-beam current which passed through the foil stack was monitored with a thin, large-area plastic scintillation detector which intercepted the electrons in the dump hole. The scintillation detector was calibrated with a Faraday cup. Its response was measured for electron-beam currents ranging from 0.1 pA to 10 nA; the present experiments were performed with beam currents ranging from 0.01 to 10 pA.

A block diagram of the data-collection electronics is shown in Fig. 7. The multichannel analyzer (MCA) received signal pulses from a charge-sensitive amplifier connected to the x-ray detector. Coincidence gating with the electron-beam bursts eliminated extraneous background

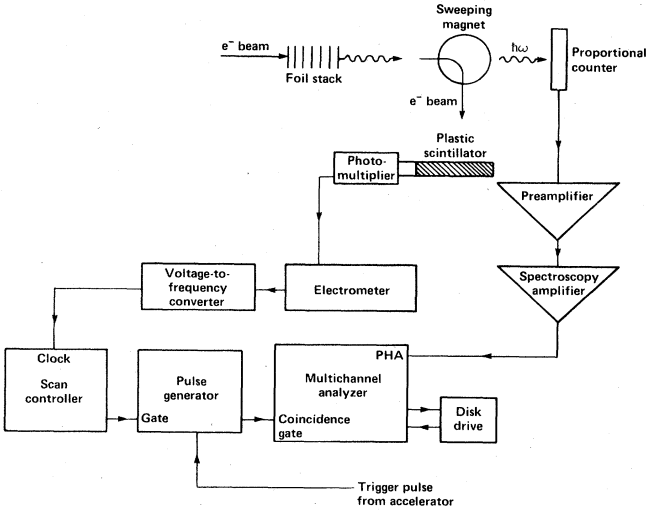

FIG. 7. Block diagram of the data-collection electronics. The electron beam was deflected by the sweeping magnet through the large-area plastic scintillator which served as the beam monitor. Coincidence gating was used, and photons were counted until a preset amount of charge had passed through the monitor. PHA is the pulse-height analyzer.

counts. Photons were counted until a fixed amount of beam charge had passed through the foil stack. This was accomplished by using a scan controller to count pulses from a voltage-to-frequency converter (VFC). The input of the VFC was the voltage output from an electrometer, which measured the output current of the beam monitor. When the desired number of VFC pulses had been received, the scan controller inhibited the coincidence pulse generator. This allowed the various spectra to be normalized to each other despite any fluctuations in the beam current.

A gas-flow proportional counter was used to detect the soft-x-ray emission. This detector had a thin (35 μg/cm^2) VYNS polyvinyl acetate window supported by a wire mesh. The x rays entered a 3×10-mm^2 slit, with the long dimension parallel to than anode wire. The counter had a 2.2-cm inside diameter. For most of the experiment the detector gas was a mixture of 90% argon and 10% propane (*P*-10 gas) at a pressure of 275 Torr. In order to observe the low-energy transition radiation from carbon as well as to obtain higher efficiency at $\simeq$3 keV, the *P*-10 gas was replaced by 90% neon and 10% propane, also at 275 Torr.

The detector system was calibrated using an ^{55}Fe radioactive source, which emits 5.89-keV x rays. The 2.89-keV argon escape peak also was observable and was used for calibration of the MCA. The resolution of the detector was measured, using the ^{55}Fe source, to be 12.5% at 5.89 keV and was assumed to vary inversely with the square root of the photon energy. The data presented in the following section were divided by calculated detector efficiencies which also accounted for photon absorption in the window.

The detector could be translated over a distance of 14 cm. The direction of motion was perpendicular to the beam line, allowing the transition-radiation cone to be scanned as shown in Fig. 8. A small shift Δy of the detector slit relative to the horizontal axis of the beam line effectively narrowed the observed radiation cone. This was corrected in the analysis of the data. The maximum angle of emission that could be measured was approximately 33 mrad and was defined by the 10-cm-diam beam pipe.

The counting rate was kept below 0.1 event per electron-beam pulse in order to reduce the registration of sum pulses (two or more events occurring during the same beam pulse). The pulse-repetition frequency of the linac was 1440 Hz; thus, in 10—15 min we were able to acquire spectra with good statistics.

Three radiator stacks, of beryllium, carbon, and aluminum, were used during the experiment. The diameters of these foils were 1, 2.54, and 1 cm, respectively. The 1.0-μm-thick metal foils of beryllium and aluminum were mounted on spacers 1.5 mm thick, while the 1.0-μm-thick carbon foils were mounted on 0.75-mm-thick spacers. These dimensions were chosen to maintain adequate support of the delicate foils and to prevent flexure.

A special stack of 28 Mylar foils of thickness 1.5 μm also was constructed in order to obtain enhanced emission in half of the radiation cone, as shown in Fig. 5(a). The Mylar was stretched over half of a 2.54-cm-diam hole, as shown in Fig. 5(b). The spacing between the foils was 5 mm. Mylar was used because it is durable and does not tear easily when stretched.

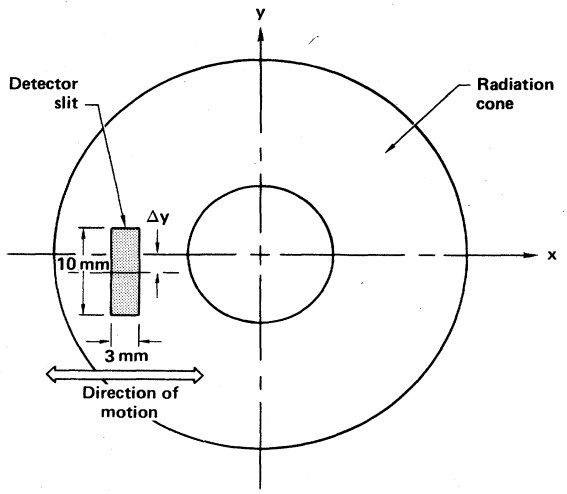

FIG. 8. Position of the detector slit relative to that of the radiation cone. The detector was translatable in the horizontal (x-axis) direction, but not in the vertical (y-axis) direction. Thus, a small vertical displacement Δy of the slit position relative to that of the horizontal plane of the radiation cone occurred, and the calculated values for the cone angle had to be adjusted accordingly (see text).

IV. EXPERIMENTAL RESULTS

A. Photon-energy spectra

The raw data for the beryllium-foil stack at 54 MeV are presented in Fig. 9. The two spectra shown were obtained with and without the 127-μm aluminum foil present (see Fig. 6 and the discussion in the preceding section). With the 127-μm foil inserted, the soft transition radiation was blocked and a background spectrum was obtained. The background spectra measured in this way were subtracted

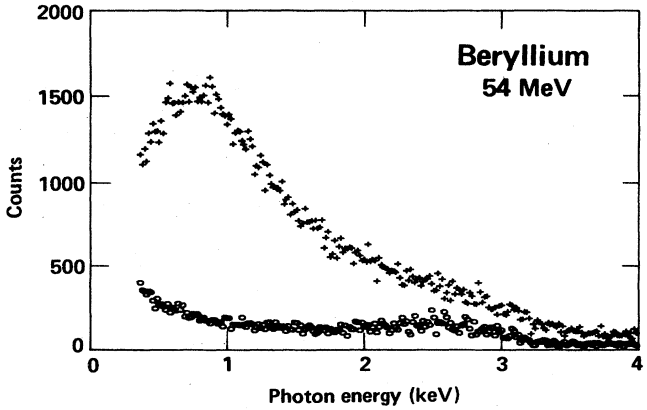

FIG. 9. Experimental energy spectra from a stack of 18 beryllium foils. The lower data points (circles) represent background radiation obtained when the 127-μm aluminum foil blocked the soft-x-ray flux. The data have been corrected for the variation with photon energy of the detector efficiency.

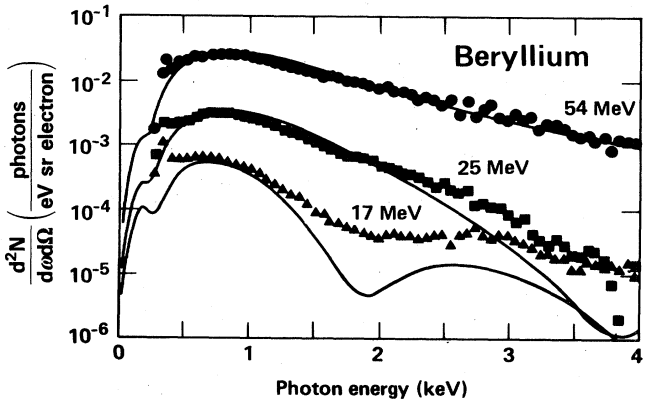

FIG. 10. Measured absolute differential production efficiencies for transition radiation emitted by an 18-foil beryllium stack for incident electron-beam energies of 54, 25, and 17.2 MeV. The calculated curves are corrected for detector resolution. The detector noise threshold was 0.4 keV.

to obtain the data presented here. The background in every case was small, as can be seen from this example.

The absolute differential production efficiencies for transition radiation from an 18-foil beryllium stack for 54-, 25-, and 17.2-MeV incident electrons are shown in Fig. 10 and are compared with the curves calculated with Eq. (9). Since the data have been plotted on a logarithmic scale, the radiation peaks seem less pronounced than those shown in the calculated linear plots of Fig. 3. The slight deviation from the calculated values on the low-energy side of the spectrum is probably attributable to uncertainty in the background subtraction at very low photon energies. For the 17.2- and 25-MeV electrons, the larger discrepancies seen above 2 keV also can be attributed to the same effect. Elsewhere, the data match the calculated values within the uncertainty of the measured incident electron flux, typically 5%.

The absolute differential production efficiencies for transition radiation from a stack of 18 carbon foils for electrons of 54, 25, and 17.2 MeV also were measured and

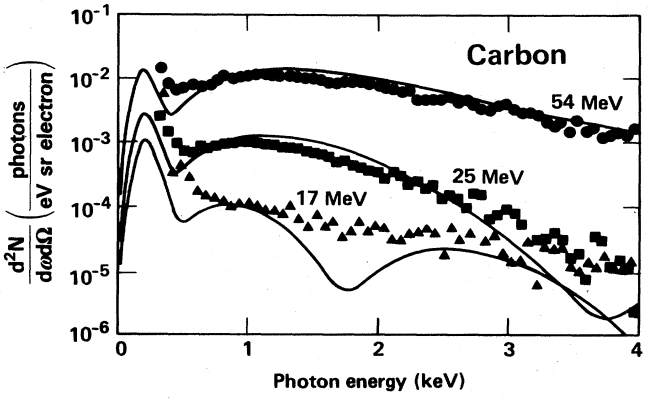

FIG. 11. Measured absolute differential production efficiencies for the transition radiation emitted by an 18-foil carbon stack for incident electron-beam energies of 54, 25, and 17.2 MeV. The calculated curves are corrected for detector resolution. The detector noise threshold was 0.4 keV.

are compared with calculated curves in Fig. 11. The accuracy with which the experimental data match the calculated values verifies the coherence effect between single-foil interfaces predicted by Eq. (5).[12]

Both Figs. 10 and 11 show the dependence of the emission intensity per unit solid angle upon electron energy. The radiation intensity near 1 keV decreases by roughly a factor of 10 when the electron-beam energy decreases by a factor of 2. Also, the emission decreases rapidly as the photon energy exceeds the critical frequency $\gamma\hbar\omega_2$.

For most of these measurements, the noise threshold was 0.4 keV, and the 270-eV peak in the carbon spectrum could not be observed. In order to observe this peak the noise threshold was lowered to 0.2 keV by using the second gas mixture, of propane and neon, which provided higher gain. In the resulting spectrum, shown in Fig. 12(b), the high-energy side of the carbon K-edge peak is

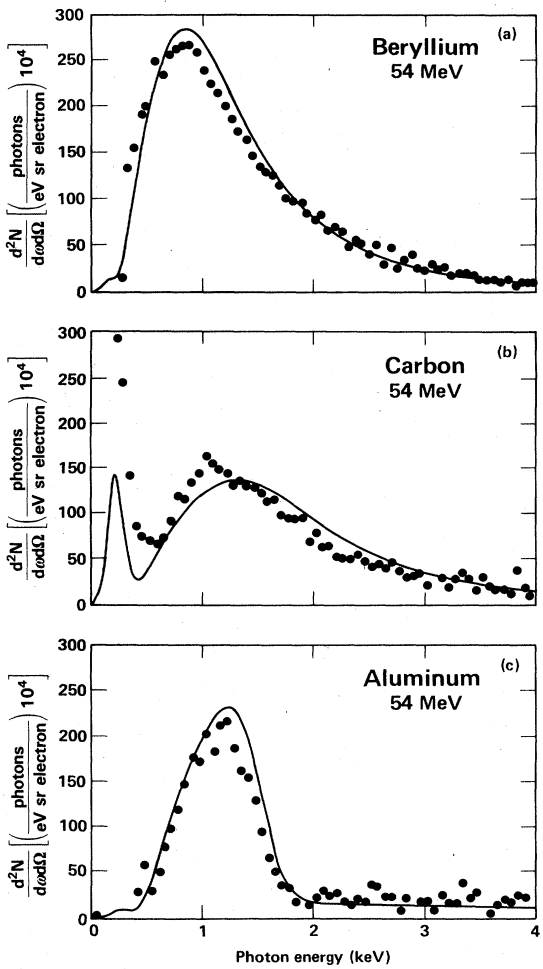

FIG. 12. Experimental results on the effect of K-shell photoabsorption on transition radiation. The carbon (b) and aluminum (c) spectra show effects of K-shell photoabsorption with edges at 284 and 1560 eV, respectively. The beryllium (a) spectrum does not extend low enough in energy to show the effect of its K-shell absorption edge at 104 eV. The parameters of the foil stacks are given in Table I. The electron-beam energy was 54 MeV. The noise threshold of the detector was 200 eV for the carbon and aluminum measurements (see text).

TABLE I. Parameters of the foil stacks and the experimental results.

Foil material	l_2 (μm)	l_1 (mm)	$\hbar\omega_2$ (eV)	M	K edge (eV)	$\hbar\omega_{peak}$ (eV)	FWHM $\hbar\omega_{peak}$
				54 MeV			
Be	1.0	1.5	24.5	18	111	800±20	1.39±0.03
C	1.0	0.75	27.0	18	284	1300±20	1.20±0.03
Al	1.0	1.5	31.0	30	1560	1300±20	0.67±0.03
				25 MeV			
Be	1.0	1.5	24.5	18	111	800±20	1.18±0.05
C	1.0	0.75	27.0	18	284	1000±30	1.33±0.05
Al	1.0	1.5	31.0	30	1560	1000±15	0.95±0.05
				17.2 MeV			
Be	1.0	1.5	24.5	18	111	975±50	0.92±0.04
C	1.0	0.75	27.0	18	284	1115±50	0.88±0.04
Al	1.0	1.5	31.0	30	1560	1100±30	0.88±0.03

seen clearly. This spectrum is compared with the measured beryllium and aluminum spectra in Figs. 12(a) and 12(c), respectively.

Figure 12(c) shows the effect of photon absorption above the K edge of aluminum at 1.56 keV. Since the detector resolution is low, the abrupt increase in absorption is smoothed in the measured spectrum. The spectra shape and the absolute differential production efficiency for each of the three foil stacks are well matched by the calculated curves. The physical parameters and the experimental results at 54 MeV for all three stacks are summarized in Table I. (Note in Table I that $\hbar\omega_{peak}$ is the measured photon energy of the radiation peak and FWHM is the full width at half maximum of that peak.)

B. Angular distributions

As illustrated schematically in Fig. 1, the angular distribution of the flux from a transition radiator is conical in shape and is a function of both the plasma frequency of the foil material and the electron-beam energy. For ultrarelativistic electrons ($\gamma \gg 1$), the peak angle is $\theta_{opt} \simeq 1/\gamma$; however, for medium-energy electron beams (as were used in this work) the optimum angle of emission must be computed from Eq. (4). The angular distribution of the radiation, for each of the three incident electron energies, was obtained by scanning the photon detector perpendicular to the beam direction.

The results for beryllium are shown in Fig. 13. The number of counts from 661 to 1000 eV for the 54- and 25-MeV cases and from 506 to 5000 eV for the 17.2-MeV case plotted. In order to match the calculated values to the experimental data, Eq. (9) was integrated over the stated bandwidth and over the solid angle subtended by the detector slit. The calculated values also were corrected to include the vertical shift Δy of the position of the slit relative to that of the horizontal plane of the radiation cone, which was obtained by normalizing the peak-to-valley ratios of the calculated curves to the experimental ones. Because of changes in linac operating conditions this varied from one run to the next, as shown in Table II. The curves so calculated, also shown in Fig. 13, match the ex-

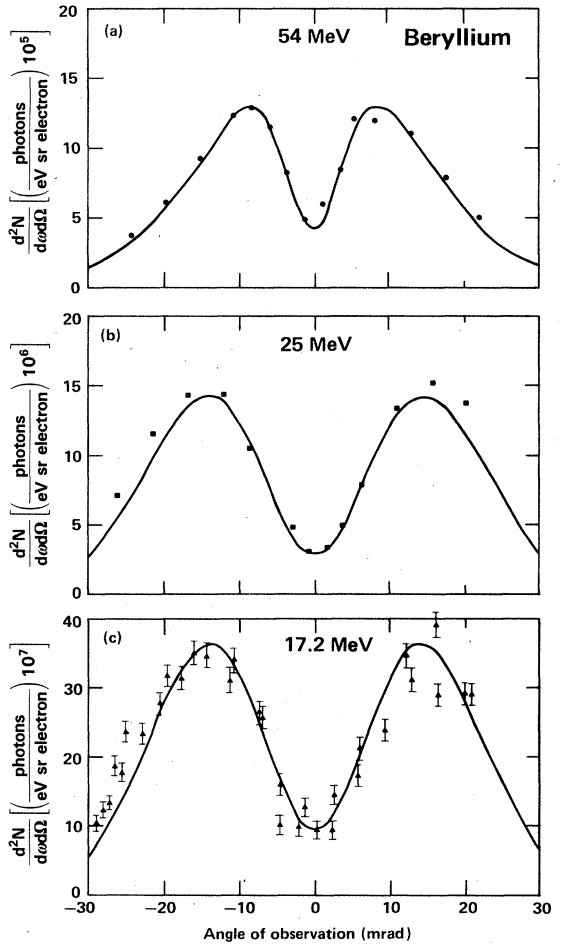

FIG. 13. Measured angular distributions of transition radiation emitted from an 18-foil beryllium stack for incident electron-beam energies of 54, 25, and 17.2 MeV. The statistical uncertainties are shown as error flags for the 17.2-MeV case (c); for the 54- and 25-MeV cases [(a) and (b)], the magnitude of the statistical uncertainties was smaller than the plotted symbols.

TABLE II. Comparison of measured and calculated values of the angle of maximum emission for the three electron-beam energies using the beryllium-foil stack.

Energy (MeV)	$1/\gamma$ (mrad)	θ_{opt} (mrad)	Bandwidth (eV)	Δy (mm)	θ_{calc} (mrad)	$(\theta\pm\Delta\theta)_{meas}$ (mrad)
54	9.4	8.2	661—1000	1.3	8.4	8.2±0.5
25	20.0	14.8	661—1000	0.2	14.3	14.8±0.5
17.2	28.9	20.0	506—5000	1.6	13.9	14.4±0.5

perimental ones well for all three cases.

Table II lists the measured angles of peak intensity $(\theta\pm\Delta\theta)_{meas}$ obtained from Fig. 13 and compares them with the values of θ_{opt} (calculated at $\hbar\omega=800$ eV), θ_{calc} (taking into account bandwidth, solid angle, and Δy), and the value of $1/\gamma$. The table shows that the values of θ_{calc} match the measured values well. The large apparent deviation from θ_{opt} for the 17.2-MeV case arises primarily from the fact that the spectrum was integrated over a very large energy interval.

C. Enhancement of transition radiation

An angular scan of the split stack of Mylar foils also was obtained using the experimental apparatus shown in Fig. 6 and the foil stack shown in Fig. 5. The beam energy was 54 MeV and the beam diameter was 2 mm. The separation between foils was 5 mm and the length of the stack was 14 cm. The number of foils was limited to 28 in order for the foil stack to fit in the target chamber. A longer stack of 100 foils or more could be constructed, which presumably would result in an increase in intensity in the upper half plane of a factor of 5 or more.

The photon flux was integrated from 534 to 5500 eV and is plotted as a function of angle in Fig. 14. The figure shows the intensity in the upper half plane to be a factor of 1.8 greater than that in the lower half plane. Thus x rays are escaping preferentially from the foil stack in the upper half plane, as one would expect.

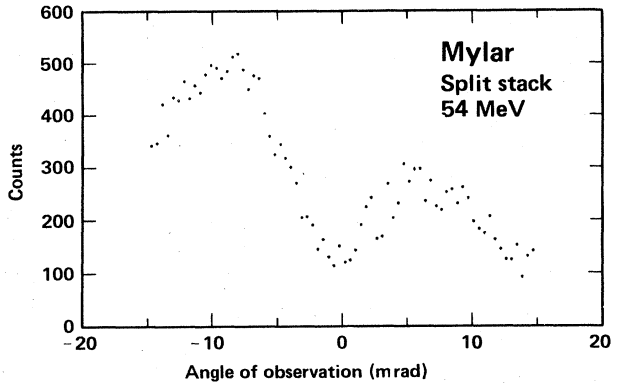

FIG. 14. Measured angular distribution of a split stack of 28 1.5-μm-thick Mylar foils. The radiation escaping from the stack in the upper half plane (the peak on the left) is larger than that from the lower half plane (the peak on the right). The energy bandwidth is given in the text.

The stack was originally designed for a 1-mm beam to produce photons at 1500 eV. The spacing for the foils was calculated to be $l_1=\gamma\, d\sigma/2\simeq 5$ mm. The electron beam was a factor of 2 larger than expected, and the spacing should have been 1 cm for 1500-eV photons. However, the results clearly show that the radiation can be enhanced in the upper half plane.

The relative spectral intensity as a function of photon energy is shown in Fig. 15. The detector was placed at an angle of 9.2 mrad for this run. Since Mylar contains carbon, the decreased photoabsorption below the K edge again results in peak at 270 eV.

V. AN X-RAY SOURCE FOR LITHOGRAPHY

Many scientific applications are possible with an intense, monochromatic, easily tunable, forward-directed, polarized x-ray source. Among them are microholography and microscopy. Perhaps the most important technological application of soft x rays will be that of submicron lithography for the production of high-density integrated circuits.[18,19] By decreasing the size of the circuit elements, the amount of circuitry that can be placed on a single silicon chip is increased. Present geometries typically have 1.5-μm-wide conducting lines. In order to produce finer lines, designers need new lithographic methods. X-ray imaging appears to be one of the more exciting possibilities. Submicron lines already have been produced with conventional x-ray sources.

Based upon several considerations, including photoresist absorption, contrast from masks, diffraction ef-

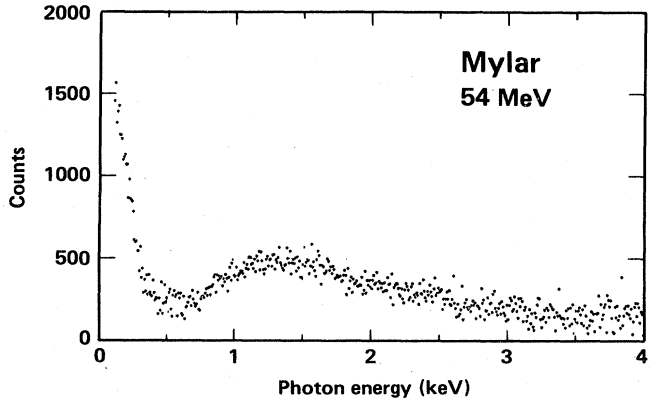

FIG. 15. Photon-energy spectrum of transition radiation from the split stack of Mylar foils. The angle of observation is 9.2 mrad in the upper half plane (see Figs. 5 and 14).

fects, and production of secondary electrons, the optimum photon-energy range is from 500 to 2500 eV. Our measurements have established that transition radiation produced with a medium-energy accelerator is strongest in just this energy band. The use of lower-energy electron beams can result in a source which is competitive with conventional and synchrotron sources.

The most common photoresist that has been used for lithography is polymethylmethacrylate (PMMA), although other resists have been developed with 10—100 times more sensitivity. The sensitivity of the photoresist is an important consideration because it determines the amount of energy per unit area that must be absorbed and therefore determines the required exposure time, a key cost factor. Higher-sensitivity materials have several disadvantages, the most important of which is their relatively low spatial resolution. In designing an x-ray lithography source a reasonable objective is an x-ray fluence of 250 mJ/cm^2, which corresponds to approximately four times the sensitivity of PMMA.

An exposure time of 20 s is considered to be sufficiently short for very-large-scale-integration fabrication, since the required handling and positioning time is at least several seconds. For a sensitivity of 250 mJ/cm^2, the corresponding power density is 12.5 mW/cm^2. A water-cooled rotating-anode bremsstrahlung source can produce about 5 W/cm^2 sr in the useful photon-energy range, which gives a power density of $\simeq$0.2 mW/cm^2 at a distance of 50 cm from the anode. This power density is a factor of 60 lower than is needed. Synchrotron-radiation sources can meet the desired intensity, but the requisite high-energy accelerators are large and expensive machines, and accessibility to them is limited.

Using a 100-MeV accelerator with an average current of 600 μA, a beryllium-foil stack of 60 foils would produce the required 12.5 mW/cm^2 at a distance of 1 m from the foil stack. Assuming that the foils lose heat only through radiation, the foil would reach a temperature of only 960 °C for a 2-mm-diam electron beam, which is well below the beryllium melting point of 1278 °C. Thus, the generation of a soft-x-ray beam suitable for lithography might very well be feasible, since both electron and hard-x-ray backgrounds are small. The prospect becomes even more attractive if and when better x-ray resists are developed.

VI. CONCLUSION

We have measured the absolute differential production efficiency and angular distribution of transition radiation from each of a variety of foil materials, and we have shown that relativistic electrons of moderately low energies can produce intense transition radiation. Our experimental values show that the fundamental formulas, as presented here and in Refs. 1—3 and 8—11, can be used to predict the salient properties of soft-x-ray emission for medium-energy electron beams. The data also show that there is coherence between single-foil interfaces. This raises the emission intensity by a factor of approximately 2 over the values that would be predicted from purely random emission from each interface. Some bandwidth narrowing associated with K-edge absorption was observed. For the aluminum stack, this resulted in narrowing of the x-ray spectrum of about 70% when compared with that for a beryllium stack, whose spectrum does not encompass its K absorption edge. For the case of the carbon stack, a sharp peak at 270 eV results from the presence of the K edge at 284 eV. Also, transition radiation was shown to be enhanced by a scheme that allows part of the radiation cone to leave the stack before very many foils have been encountered. Finally, transition radiation has many potential applications. One of the most important, x-ray lithography, was examined briefly and was judged to be feasible under appropriate conditions.

ACKNOWLEDGMENTS

The authors are pleased to acknowledge N. Peterson for the construction of the detector chamber and its translation system and G. R. Leipelt (recently deceased) for assistance with the photon detector system. This work was performed at Lawrence Livermore National Laboratory under the auspices of the U.S. Department of Energy under Contract No. W-7405-ENG-48 and was sponsored in part by the U.S. Office of Naval Research under Contract No. N00014-78-C-0403.

[1]V. L. Ginzburg and I. M. Frank, J. Phys. (Moscow) **9**, 353 (1945).

[2]G. M. Garibyan, Zh. Eksp. Teor. Fiz. **33**, 1403 (1958) [Sov. Phys.—JETP **6**, 1079 (1958)].

[3]M. L. Ter-Mikaelian, Nucl. Phys. **24**, 43 (1961).

[4]A. I. Alikhanyan, F. R. Arutyanyan, K. A. Ispiryan, and M. L. Ter-Mikaelian, Zh. Eksp. Teor. Fiz. **41**, 2002 (1961) [Sov. Phys.—JETP **14**, 1421 (1962)].

[5]L. C. L. Yuan, C. L. Wang, H. Uto, and S. Prunster, Phys. Lett. **31B**, 603 (1970).

[6]A. I. Alikhanian, S. A. Kankanian, A. G. Oganessian, and A. G. Tamania, Phys. Rev. Lett. **30**, 109 (1973).

[7]M. L. Cherry, D. Muller, and T. A Prince, Nucl. Instrum. Methods **115**, 141 (1974).

[8]A. N. Chu, M. A. Piestrup, T. W. Barbee, Jr., R. H. Pantell, and F. R. Buskirk, Rev. Sci. Instrum. **51**, 597 (1980).

[9]A. N. Chu, M. A. Piestrup, R. H. Pantell, and F. R. Buskirk, J. Appl. Phys. **52**, 22 (1981).

[10]A. N. Chu, M. A. Piestrup, T. W. Barbee, Jr., and R. H. Pantell, J. Appl. Phys. **51**, 1290 (1980).

[11]M. A. Piestrup, P. F. Finman, A. N. Chu, T. W. Barbee, Jr., R. H. Pantell, G. A. Gearhart, and F. R. Buskirk, IEEE J. Quantum Electron. **QE-19**, 1771 (1983).

[12]P. J. Ebert, M. J. Moran, B. A. Dahling, B. L. Berman, M. A. Piestrup, J. O. Kephart, H. Park, R. K. Klein, and R. H. Pantell, Phys. Rev. Lett. **54**, 893 (1985).

[13]M. L. Ter-Mikaelian, *High Energy Electromagnetic Processes in Condensed Media* (Wiley-Interscience, New York, 1972), Chaps. 4 and 5, and related bibliography.

[14]M. L. Cherry, G. Hartman, D. Muller, and T. A. Prince,

Phys. Rev. D **10**, 3594 (1974).
[15]C. W. Fabjan and W. Struczinski, Phys. Lett. **57B**, 483 (1975).
[16]A. N. Chu, M. A. Piestrup, P. F. Finman, R. H. Pantell, and R. A. Gearhart, IEEE Trans. Nucl. Sci. **NS-29**, 336 (1982).
[17]P. F. Finman, M. A. Piestrup, R. H. Pantell, and R. A. Gearhart, IEEE Trans. Nucl. Sci. **NS-29**, 340 (1982).
[18]D. L. Spears and H. I. Smithe, Electron. Lett. **8**, 102 (1972).
[19]A. R. Neureuther, in *Synchrotron Radiation Research,* edited by H. Winick and S. Doniach (Plenum, New York, 1980), p. 223.